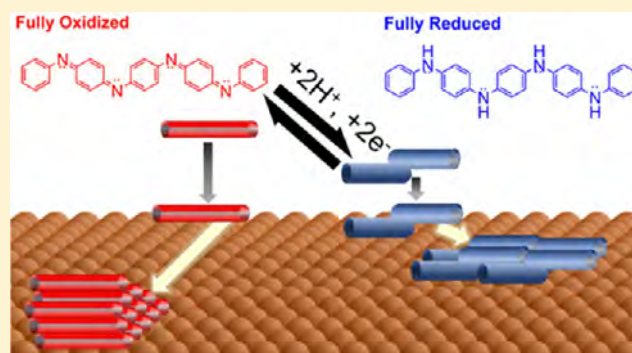


# Surface Mobility and Nucleation of a Molecular Switch: Tetraaniline on Hematite

Amirmasoud Mohtasebi,<sup>†</sup> Tanzina Chowdhury,<sup>†</sup> Mark C. Biesinger,<sup>‡</sup> and Peter Kruse<sup>\*,†</sup><sup>†</sup>Department of Chemistry and Chemical Biology, McMaster University, 1280 Main Street West, Hamilton, Ontario L8S 4M1, Canada<sup>‡</sup>Surface Science Western, Room LL31, 999 Collip Circle, London, Ontario N6G 0J3, Canada

## Supporting Information

**ABSTRACT:** Understanding the dynamics of organic thin film formation is crucial to quality control in organic electronics and smart coatings. We have studied the nucleation and growth of the reduced and the oxidized states of phenyl-capped aniline tetramer (PCAT) deposited on hematite(1000) surfaces by physical vapor deposition. The fully reduced PCAT molecules form 2D islands on the surface, whereas the fully oxidized molecules form 3D islands. Through scaled island size distribution, it was found that the critical island sizes,  $i$ , for the reduced and oxidized molecules are  $i = 4$  and  $5$ , respectively. From the dependence of the island density on substrate temperature, the activation energies for the diffusion of the molecules away from the critical cluster were calculated to be 1.30 and 0.55 eV, respectively. At low temperatures, the reduced and the oxidized PCAT molecules form compact islands on the surface. At higher temperatures, the reduced islands become dendritic, whereas the oxidized islands become slightly dendritic. The attempt frequencies for surface diffusion of the reduced and the oxidized islands were estimated to be about  $5 \times 10^{25}$  and  $8 \times 10^{11} \text{ s}^{-1}$ , respectively. The former value is in line with the high degree of surface wetting by the reduced PCAT, whereas the latter value shows the higher degree of intermolecular interaction in the fully oxidized PCAT and the low degree of its interaction with the iron oxide surface. Interconversion between oxidized and reduced islands through exposure to a reducing environment, and its impact on island morphology was examined. We also found that the presence of  $\text{Fe}^{2+}$  defects on the hematite surface did not impact the nucleation and growth of the molecular islands, likely due to a discrepancy in time scale. This study elucidates the interactions between an oligoaniline-based molecular switch (PCAT) and hematite surfaces as a function of molecular oxidation state, with applications in molecular electronics, chemical sensors, and smart coatings.



## INTRODUCTION

Organic thin films are key components of various electronic devices. They function as the donor/acceptor layer in organic photovoltaic devices,<sup>1</sup> as the conductive channel in thin film transistors,<sup>2</sup> and as the sensing material in chemical sensors.<sup>3,4</sup> The molecular orientation and packing plays an important role in the function of these devices as the quality of the organic thin films influences properties such as electrical conductivity or charge carrier mobility.<sup>2,5</sup> Therefore, understanding the organic thin-film formation is important for the design of better organic electronic devices and smart coatings. One of the primary steps in organic or inorganic film formation is onset of nucleation and growth of thin films.<sup>6</sup> Various studies have shown that the nucleation and growth of the organic thin films follow different behaviors than the metallic thin films. In general, the metallic islands on surfaces held at room temperature form dendritic morphologies and at higher temperatures transform into compact islands. On the contrary, the islands of many large organic molecules form compact morphologies when the substrate is at low temperature and form dendritic islands at

higher temperatures.<sup>7,8</sup> Thus the models commonly used to describe the former case<sup>9</sup> are unable to fully describe the early stages of nucleation and growth of the organic films.<sup>8</sup> One of the proposed reasons for these opposite trends is the difference in intermolecular interactions in the organic films in comparison with the metallic films.<sup>10</sup> Another reason is the intrinsic anisotropy associated with the organic molecules in contrast to the isotropy of the metal atoms.<sup>10</sup> In addition, even different oxidation states of an organic molecule can adsorb on a surface with different conformations and in different orientations.<sup>11,12</sup> This becomes important in applications such as organic electronic devices, which require a thin and homogeneous molecular layer.<sup>8</sup> For example, it has been shown that a vertical crystal of a tetraaniline can reach an electrical conductivity of 12.3 S/cm, whereas its horizontally

Received: August 15, 2017

Revised: November 3, 2017

Published: November 9, 2017

oriented crystal shows electrical conductivity values as low as  $10^{-4}$  S/cm.<sup>5</sup>

One of most studied tetraaniline molecules is the phenyl-capped aniline tetramer (PCAT), a redox-active oligomer of polyaniline (PANI) that mimics many characteristics of this polymer.<sup>13</sup> Similar to PANI it has three oxidation states and becomes electrically conductive through chemical doping.<sup>5</sup> The reversible conversion of different oxidation states of PCAT (or PANI) to each other makes it attractive for different applications such as carbon nanotube field-effect transistors with switchable polarity<sup>14</sup> or resettable chemical sensors.<sup>4</sup> In all of these applications and many others,<sup>15</sup> the interaction of the thin organic film with a substrate is crucial for the device performance and thus requires a high quality of the organic coating. The structure of the tetraaniline films on surfaces prepared through drop-casting or vapor infiltration has been studied previously.<sup>5,16</sup> It has been shown that the solvent, substrate, and the doping/undoping of the oligoaniline can significantly change the morphology, packing, and electrical conductivity of the fabricated organic film.<sup>5,16</sup> Another application of PCAT molecular layers is their use as active coatings against corrosion of metals, particularly iron-based alloys.<sup>17,18</sup> This is based on the idea that redox-active molecules in their oxidized form while in contact with the metallic substrate can provide sufficient polarization potential to form a passive oxide layer at the interface with the metallic substrate.<sup>19</sup> As a result of this process, the organic molecule is reduced, and the oxide layer protects the metal from corrosion. The reoxidation of these molecules under ambient conditions maintains the passive metal oxide film for prolonged protection of the substrate.<sup>17</sup> This reemphasizes that the key to the success of such applications is the quality of the thin-film formation on the substrate.

To understand the film formation of small organic molecules (including PCAT) on a solid surface, the early stages of this process, namely, the nucleation and growth of organic islands, should be understood. These islands are in direct contact with the underlying substrate and dictate the growth and morphology of the next monolayers.<sup>11</sup> A common method to obtain nucleation and growth parameters on the surface is through thermal desorption spectroscopy.<sup>8,11</sup> An alternative method for finding such parameters is through determination of the island size distribution by scanning probe microscopy.<sup>20</sup> This is followed by the determination of scaling island size distribution through a scaling law. On the basis of this scaling law, the size distribution of islands per unit area scales with average islands size and can therefore be reduced to a dimensionless function.<sup>20</sup> On the basis of this function, the critical number of monomers for the formation of a stable island can be evaluated. More diffusion properties such as the attempt frequency and the activation energy for diffusion of the molecules away from the critical cluster ( $E_a$ ) can be found through the study of island formation on the surface at different substrate temperatures.<sup>8</sup>

Here we study the nucleation and growth of films of PCAT in two oxidation states (fully reduced (LB) and fully oxidized (PB)) on the surface of hematite. This system is used as a model system for the commercial systems based on redox-active organic thin films on metal oxide surfaces. Using island size distribution and scaling island size distribution, the critical island sizes ( $i$ ) for the reduced and the oxidized oxidation states of PCAT were determined. The shape, morphology, surface coverage, and nucleation density of each state at various

substrate temperatures were quantified and used to determine  $E_a$  and the frequency factor for the diffusion of each oxidation state. These values can be used as a quantitative measure of mobility and wetting of the surface of iron oxide by different oxidation states of PCAT. Using a flat hematite single crystal provides an opportunity to evaluate the diffusion parameters with minimum interference from surface roughness or grain boundaries. The impact of switching the oxidation state of already deposited islands on their morphology was investigated. Finally, the chemistry of the surface of the substrate was modified through vacuum annealing without affecting the surface roughness. This was used to investigate the effect of oxidation states of the substrate on the critical island size of each oxidation state of PCAT.

## ■ EXPERIMENTAL DETAILS

PCAT was synthesized based on a literature procedure.<sup>21</sup> The preparation of the fully reduced and the fully oxidized forms of the PCAT free base was performed using the reducing and the oxidizing agents as previously described.<sup>17</sup> Natural sourced hematite(1000) single crystals were obtained from SurfaceNet. The single crystals are chemical-mechanically polished to have a final RMS roughness better than 6 Å over  $20 \times 20 \mu\text{m}^2$ . Organic thin films were deposited on substrates in a homemade vacuum chamber with a base pressure better than  $4 \times 10^{-6}$  Torr using a low-temperature Knudsen cell with a glass crucible. The sample holder can be cooled or heated in the range of 0–70 °C. Single-crystal substrates were clamped between two sapphire washers in a commercial sample holder (RHK) equipped with a heater made of tungsten wire. The substrate temperature was controlled using a temperature controller (Lakeshore Cryotronics) connected to a Ni-NiCr thermocouple clamped between the sample, and a copper sheet was placed underneath the sample. The temperatures of the hematite single crystals during the organic deposition process (20–60 °C) are kept well below the threshold required for evaporation of PCAT (above 110 °C). Using X-ray photoelectron spectroscopy (XPS), it was previously shown that the vacuum deposition under these conditions does not impact the oxidation states of PCAT (LB and PB) nor does it cause degradation of the organic films.<sup>17</sup> The deposition rate was monitored using a quartz crystal microbalance (Inficon, XTC) that is positioned next to the sample holder. In all experiments, the deposition rates were kept close to  $\sim 0.01$  nm/s.

All samples were transferred to an ex situ atomic force microscope (AFM, Veeco Enviroscope with a MultiMode IIIa controller) within 5 min of the deposition of the organic thin films. All AFM measurements were performed in a dry nitrogen environment and in tapping mode using antimony-doped Si cantilevers (Bruker, model NCHV-A) with 320 kHz resonance frequency and a maximum tip radius of 10 nm. All AFM images were analyzed using Gwyddion software.<sup>22</sup> In all AFM images the false color ruler is shown beside the topography image. Using this software, for all images the data were leveled by mean plane subtraction. The polynomial background of all images was removed with horizontal and vertical polynomial degree of 2. If necessary, scares in images were removed using the “correct horizontal scares” function of the software. Three or more samples of each oxidation state of PCAT (different coverages) deposited on hematite have been used for the scaling island size distribution analysis. For each sample, at least four AFM images have been acquired at different locations of each surface and used to collect statistics. Raman spectra of

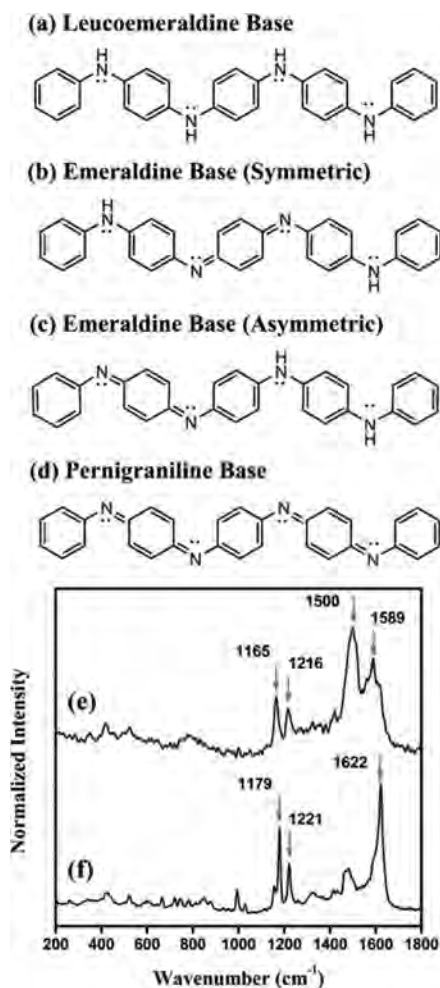
PCAT powders were acquired using a Renishaw InVia Raman spectrometer with a spectral resolution of  $2\text{ cm}^{-1}$  and an  $\text{Ar}^+$  ion laser at  $514\text{ nm}$  ( $2.41\text{ eV}$ ). The powders were dispersed in methanol and drop cast and dried on clean silicon wafers. The  $\text{NaBH}_4$  used for the production of hydrogen gas was purchased from Sigma-Aldrich.

XPS was performed using a Kratos Axis Ultra DLD spectrometer with a monochromatic  $\text{Al K}\alpha$  X-ray source ( $15\text{ mA}$ ,  $1486.6\text{ eV}$ ). The approximate analysis areas for both survey and high-resolution spectra were  $300 \times 700\ \mu\text{m}^2$ . For the former and the later measurements, pass energies of  $160$  and  $20\text{ eV}$  were used, respectively. The in situ annealing of the hematite single crystal was performed in the XPS analysis chamber with a base pressure better than  $1 \times 10^{-8}\text{ Torr}$ . The sample was heated radiatively and the annealing process was dynamically monitored by XPS. For each cycle of annealing the temperature was ramped to  $350\text{ }^\circ\text{C}$  and kept at this temperature for  $5\text{ min}$ . Then, the sample was cooled in vacuum and was stored in a dry argon environment for  $24\text{ h}$  before it was load-locked back into the XPS analysis chamber for further measurements. For each step, in addition to the survey spectra, the high-resolution ( $0.1\text{ eV}$  resolution)  $\text{C 1s}$ ,  $\text{O 1s}$ , and  $\text{Fe 2p}$  spectra were acquired. CasaXPS software (version 2.3.17) was used for analysis of XPS spectra.<sup>23</sup> Shirley-type background and line-shape of  $\text{GL}(30)$  were used for all peak integrations. All spectra were charge corrected to the binding energy (BE) of  $284.8\text{ eV}$  for  $\text{C-C}$  and  $\text{C-H}$ .

## RESULTS AND DISCUSSION

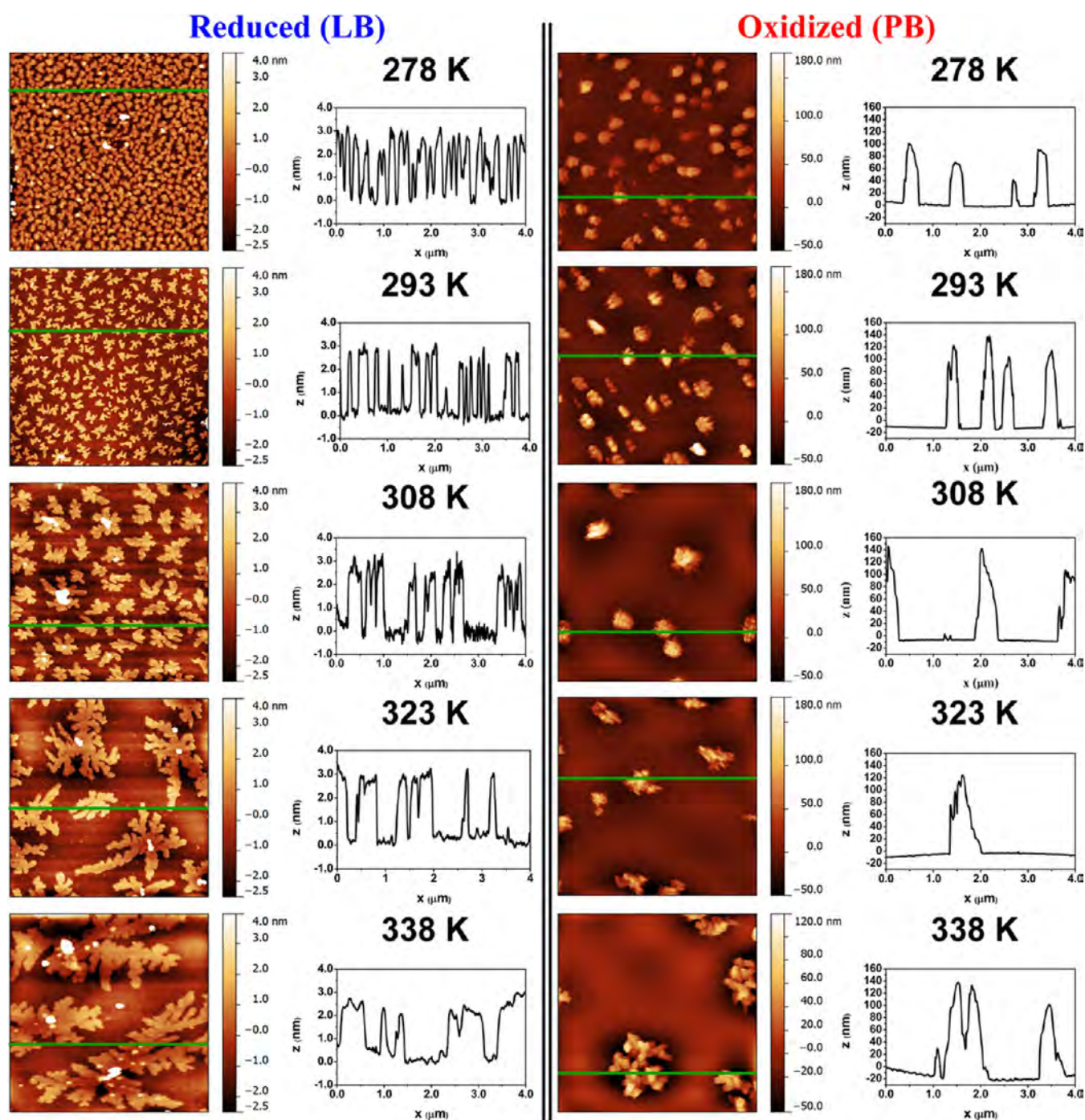
PCAT in its base form (undoped) can be prepared in three different oxidation states: fully reduced, half oxidized, and fully oxidized.<sup>17</sup> The molecular structure of each state is depicted in Figure 1a–d. The fully reduced (Figure 1a) and the fully oxidized (Figure 1d) forms of PCAT can be prepared using excess amount of a reducing agent (e.g., L-ascorbic acid) and an oxidizing agent (e.g., ammonium persulfate), respectively. Commonly, the preparation of the half oxidation state of PCAT is performed through the addition of 1:1 molar ratio of ammonium persulfate to fully reduced PCAT with the hope to create an exact half oxidation state of the oligoaniline.<sup>17</sup> However, it is known that there is poor control over the final oxidation states of the molecules achieved through this procedure.<sup>24</sup> In addition, using scanning tunneling microscopy (STM), it has been shown that submonolayer films of vacuum-deposited half-oxidized PCAT on the surface of  $\text{Cu}(110)$  show disordered structures.<sup>25</sup> This behavior has been attributed to the multiple isomers of this oxidation state of PCAT (Figure 1b,c).<sup>25</sup> The same conclusion was also arrived at using nuclear magnetic resonance spectroscopy of this oxidation state.<sup>26</sup> Therefore, the focus of this work is only on the nucleation and growth of the fully reduced and the fully oxidized PCAT, which can be prepared with high precision. The oxidation states of the former and the latter oligoanilines prepared through chemical redox processes were examined by Raman spectroscopy. The Raman spectrum of the fully reduced form (Figure 1f) shows the main bands at  $1179$ ,  $1221$ , and  $1622\text{ cm}^{-1}$ , an indication of a successful reduction process. The Raman spectrum of the oxidized form (Figure 1e) shows the bands at  $1165$ ,  $1216$ ,  $1500$ , and  $1589\text{ cm}^{-1}$  in agreement with the Raman bands of the fully oxidized PCAT.<sup>27</sup>

Figure 2 shows the evolution of the morphologies of the fully reduced and the fully oxidized PCAT on the surface of a hematite(1000) single crystal as a function of surface



**Figure 1.** Molecular structure of different oxidation states of base PCAT: fully reduced (a), half-oxidized symmetric isomer (b), half-oxidized asymmetric isomer (c), and fully oxidized (d) states. Raman spectra of the fully oxidized (e) and the fully reduced (f) base PCAT.

temperature. At a low substrate temperature ( $278\text{ K}$ ), high densities of the reduced and the oxidized islands with nearly compact morphologies can be found on the surface. By increasing the substrate temperature, the density of the reduced islands decreases while the islands become more dendritic but with smooth corners. Regardless of the temperature, for all fully reduced islands their cross-section profiles show an island height of  $\sim 3\text{ nm}$  (Figure 2). This dimension is close to the length of PCAT molecules ( $\sim 2.3\text{ nm}$ ), as measured by STM and evaluated by DFT calculations.<sup>25</sup> At surface temperatures above  $323\text{ K}$ , the main dendritic islands are surrounded by small islands/nuclei with identical sizes. The same behavior has been previously reported for hexaphenyl (6P) islands on amorphous mica and was attributed to the existence of not well amorphized areas of the substrate or possible surface impurities.<sup>8</sup> At higher substrate temperature ( $338\text{ K}$ ), the number of these small islands decreases. This may be due to the sufficient thermal energy present for their diffusion to the larger dendritic islands. Another reason might be the transition from a complete condensation into an incomplete condensation of the incoming flux to the surface at  $\sim 338\text{ K}$ .<sup>8</sup> This means that the sticking coefficient for the incoming molecules is  $< 1$ . Some of them stick to the surface to form islands while others are reflected back into the vacuum due to the high thermal energy



**Figure 2.** AFM images ( $4 \mu\text{m} \times 4 \mu\text{m}$ ) of the reduced (left column) and the oxidized (right column) PCAT molecules on hematite surface at different substrate temperatures (278, 293, 308, 323, and 338 K). The height cross-section of each figure extracted along the green line is represented next to each AFM micrograph.

of the surface. The growth of the fully oxidized islands on hematite surfaces as a function of temperature shows a similar trend to the fully reduced islands. However, at any temperature the density of the fully oxidized islands is lower than that of the fully reduced islands. In addition, the effect of temperature on the change in the island density of the fully oxidized islands is far less than on the fully reduced islands. At temperatures between 278 and 308 K, the islands are nearly globular. Above these temperatures, their shape starts to become slightly dendritic. The cross-section height profiles of the fully oxidized islands at different surface temperatures show somewhat similar

heights, which fluctuate between 110 and 130 nm. This behavior is an indication of far less wetting of the hematite surface by this oxidation state of PCAT in contrast with the good wetting of the same surface with LB islands. This growth mechanism in which the island shapes are compact at lower temperatures and become more dendritic at higher temperatures is opposite of what has been reported for the growth of the metallic islands.<sup>28</sup> This behavior has been previously reported for other large organic molecules such as  $6\text{P}^{10}$  and hexathiophene.<sup>7</sup> In the latter case, at low temperatures the islands are dendritic and an increase in the temperature makes

them more compact. It is known that the commonly metallic island growth follows the classical diffusion-limited aggregation model.<sup>29</sup> In this process, at low temperature, atoms stick to the nearest stable islands.<sup>10</sup> These atoms do not have enough energy to diffuse along the rim of the island, which hinders the formation of compact morphologies. However, an increase in the temperature provides enough energy for diffusion of atoms, which causes the formation of compact islands that are more thermodynamically stable.<sup>8</sup>

The kinetics of diffusion of atoms and molecules on surfaces is defined by the ratio of the diffusion constant ( $D$ ) to the incoming flux to the surface ( $F$ ). Through these parameters, other parameters of a deposition process such as nucleation density ( $N$ ) can be calculated.<sup>20</sup> These parameters are related to each other through eq 1, where  $\theta$  is the surface coverage,  $A(\theta)$  is the average island size,  $C$  is a proportionality constant, and  $\chi = i/(i + 2)$  ( $1/3 \leq \chi < 1$ ,  $i \geq 1$ ), where  $i$  is the critical island size.<sup>10,20</sup> The critical island size is the smallest number of particles (atoms or molecules) required such that by addition of one extra particle a stable island can be formed.<sup>8</sup> Once an island becomes stable, it is assured not to undergo dissociation.<sup>20</sup>

$$N = C \left( \frac{D}{F} \right)^{-\chi} \cong \frac{\theta}{A(\theta)} \quad (1)$$

It was shown that in the aggregation regime (typically  $0.1 \leq \theta \leq 0.5$ ) the island size distribution shows a scaling behavior.<sup>30</sup> The aggregation regime by definition is a range of surface coverages in which the island density remains nearly unchanged.<sup>8,20</sup> This means that the interisland length scale is the only determinantal length and thus is a sign of diffusion-mediated growth.<sup>20</sup> In diffusion-mediated growth, the distribution of islands of size  $a$  per unit area ( $N_a(\theta)$ ) scales with  $A(\theta)$  through eq 2.<sup>30</sup>

$$N_a = \theta A(\theta)^{-2} f_i(u) \quad (2)$$

In this equation,  $f_i(u)$  is a dimensionless scaling function dependent on  $i$  while  $u = a/A(\theta)$ . This function is defined based on eq 3, in which  $C_i$  and  $b_i$  are only functions of  $i$  and can be obtained numerically.<sup>8</sup>

$$f_i(u) = C_i u^i \exp(-b_i u^{1/b_i}) \quad (3)$$

Other parameters such as  $E_a$  can be obtained through combination of eqs 1 and 2 with eq 4, where  $T$  and  $R$  are the temperature and the gas constant (8.314 kJ/mol), respectively.

$$D = D_0 \exp\left(\frac{-E_a}{RT}\right) \quad (4)$$

Assuming the situation in which  $F$  and  $\theta$  are constant,  $N_a$  and  $E_a$  can be related as  $N_a \propto \exp(-E_a/RT)^{-\chi} \propto \exp(\chi E_a/RT)$ . Thus  $N_a = a_0 \exp(\chi E_a/RT)$ , where  $a_0$  is a proportionality constant that can be related to  $N_a$  and  $E_a$  through the following linear equation

$$\ln N_a = \ln a_0 + \frac{\chi E_a}{RT} \quad (5)$$

To obtain diffusion parameters of the reduced and the oxidized PCAT on the hematite surface, the nucleation density of these two species has to be measured at various temperatures. Figure 3 shows the island density as a function of temperature (278 to 338 K) for these two types of PCAT islands on hematite surface in the form of  $\ln N_a$  versus  $1/T$ . Data points of

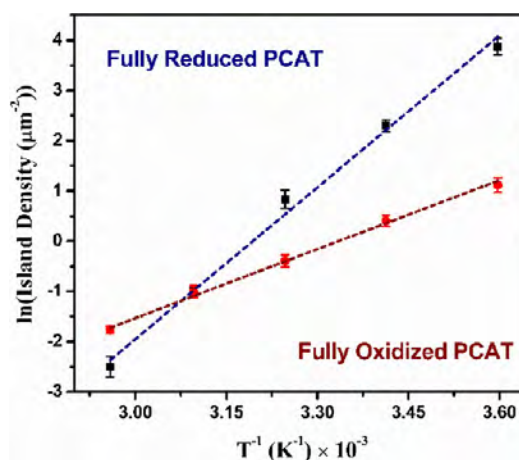
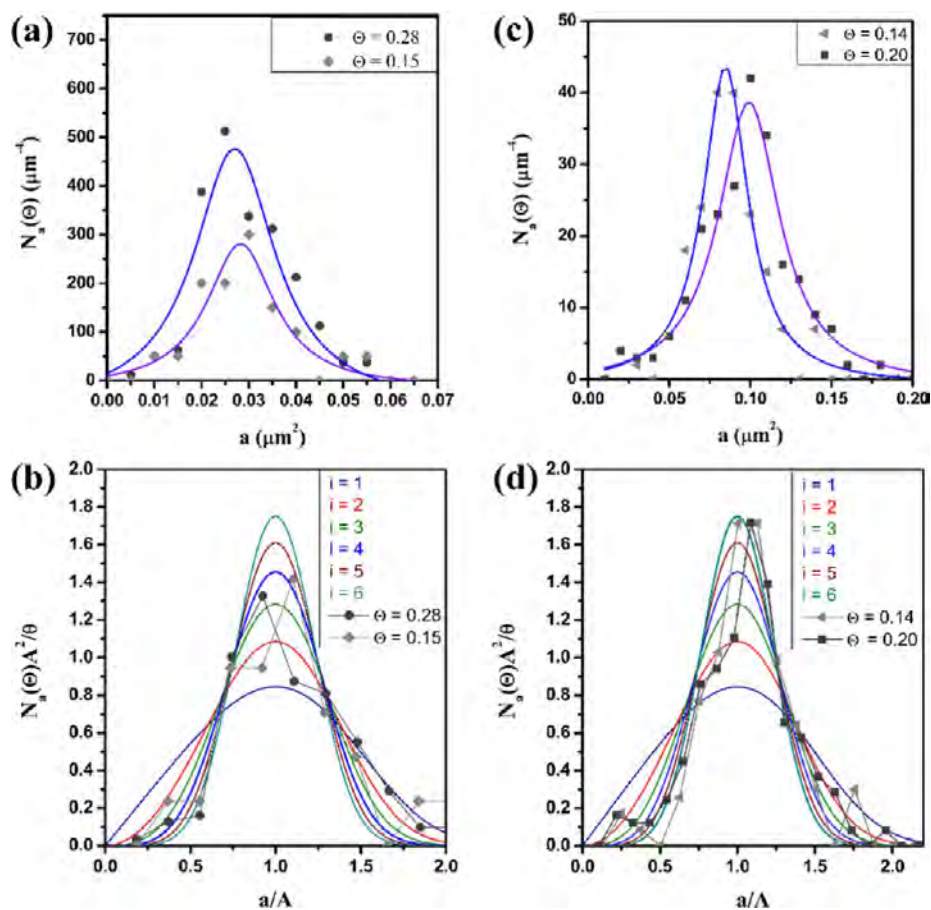


Figure 3. Island density of the fully reduced and the fully oxidized on hematite(1000) single crystal as a function of surface temperature.

each oxidation state of PCAT can be fitted with a linear line. The adjusted  $R$ -square values for the fitted line to the reduced PCAT data points and the oxidized PCAT data points are 0.993 and 0.998, respectively. The absence of any bend in these two lines at this temperature range indicates that only one growth mechanism is dominant.<sup>8,10</sup> On the basis of eq 5, the activation energies of both the reduced and the oxidized PCAT islands can be calculated using the slope of the linear fitted lines ( $\chi E_a/R$ ). Thus to obtain  $E_a$  values for each oxidation state of PCAT islands, the evaluation of  $\chi$  values is necessary. Because  $\chi = i/(i + 2)$ , the  $i$  value has to be measured for each oxidation state of PCAT. Therefore, the island size distributions of both the reduced and the oxidized islands at 293 K and at different surface coverages in the aggregation regime were measured. Aggregation regime (typically  $0.1 < \theta < 0.5$ ) is the range of surface coverages in which the island density remains nearly constant, and the island size distribution shows a scaling behavior.<sup>8,20</sup> It was ensured that all samples of the reduced and the oxidized PCAT islands on hematite are in the aggregation regime as the island density at different coverages remained nearly constant ( $11.12 \pm 0.69$  and  $2.05 \pm 0.19$ , respectively). For each coverage, the  $N_a$  has a maximum that is located at  $A(\theta)$ .<sup>20</sup> To find  $i$  for each type of island, all island size distributions are converted to  $f_i(u)$  by multiplying  $N_a$  by  $A(\theta)^2/\theta$  and dividing  $a$  by  $A(\theta)$ . This way, for each specific molecule, the island density curves at different surface coverages are scaled down to a single curve of  $f_i(u)$ .<sup>20</sup> The maximum of such curve is located around  $a/A = 1$ . Comparison of the experimentally obtained  $f_i(u)$  curves with  $f_i(u)$  curves obtained numerically for different  $i$  values through eq 3 is used to assess  $i$  values of the islands. Figure 4a,c shows the island size distribution of the reduced and the oxidized islands, respectively, each at two different surface coverages. The scaled distribution of the island size distribution curve of the reduced islands at two different coverages leads to two curves both located around  $f_i(u)$  for  $i = 4$  (Figure 4b). Considering that  $i$  has to be an integer number,<sup>8</sup> the residual sum of squares of the experimental data and  $f_i(u)$  was compared for different  $i$  values, with  $i = 4$  showing the best fit to the experiment. Therefore, five reduced PCAT molecules are required to form a stable island. The scaled distribution of the island size distribution of the oxidized islands are located close to  $f_i(u)$  for  $i = 5$  (Figure 4d), again based on a comparison of the residual sum of squares. Therefore, six oxidized PCAT molecules are required to form a



**Figure 4.** Island size distribution  $N_a(\theta)$  of the reduced (a) and the oxidized (c) PCAT islands at different surface coverages. (b) Scaled island size distribution of the island size distribution in panel a. (d) Scaled island size distribution of the island size distribution in panel c. In both panels b and d the scaling functions  $f_i(u)$  for critical cluster sizes of  $i = 1-6$  are shown along the experimentally measured data.

stable island on a hematite surface. Using the critical island size of the reduced and the oxidized islands, the  $\chi$  values will be 4/6 and 5/7, respectively. On the basis of this information and the slope of the linear fits in Figure 3, the activation energies for diffusion of the molecules away from the critical cluster for the reduced and the oxidized islands are estimated to be about 1.30 eV (125 kJ/mol) and 0.55 eV (53 kJ/mol), respectively.  $E_a$  consists of two energy terms through  $E_a = E_i + iE_d$ , where  $E_i$  is the binding energy of the critical cluster and  $E_d$  is the activation barrier for diffusion of each molecule. Although, it is not possible to find the exact values of  $E_i$  and  $E_d$  directly from the method used in this work, their sum is typically dominated by  $E_i$ .<sup>8</sup>

In addition to the information previously obtained, the attempt frequency ( $\nu_0$ ) for surface diffusion of the reduced and the oxidized islands can be calculated. This parameter can be evaluated using eq 6,<sup>8</sup> where  $y_{0T}$  is the intercept of fittings in Figure 3 with the  $y$  axis,  $\eta$  is a weak function of  $\theta$  and  $i$ ,  $N_0$  is the number of surface sites per unit area, and  $F$  is the deposition rate.

$$y_{0T} = \ln(\eta N_0) + \frac{i}{i+2} \ln\left(\frac{4}{N_0}\right) - \frac{i}{i+2} \ln \nu_0 + \frac{i}{i+2} \ln F \quad (6)$$

The main information required for evaluation of these parameters can be obtained from Figure 3 in addition to the critical island size  $i$  for each oxidation state of PCAT.  $N_0$  was

estimated to be  $\sim 4.8 \times 10^{14}$  PCAT molecules per  $\text{cm}^2$ . Considering that the reduced islands are 2D and the oxidized islands are 3D in shape, the value of  $\eta$  for both of these islands was estimated to be  $\sim 2.5$ .<sup>9</sup> Therefore, on the basis of this information the attempt frequencies for the reduced and the oxidized islands on the surface of hematite(100) were estimated to be  $5 \times 10^{25}$  and  $5 \times 10^{11} \text{ s}^{-1}$ , respectively. The attempt frequency for the reduced islands is significantly higher than the typical attempt frequency values for the surface diffusion of atoms ( $\sim 10^{11}$  to  $10^{13}$ ).<sup>9</sup> However, such large attempt frequency values are not unrealistic because similar values have been reported for other small organic molecules with similar molecular weight (6P on Au(111) and mica).<sup>8,31</sup> The high attempt frequency of 6P was explained through transition-state theory based on the fact that large organic molecules have many more translational, vibrational, and rotational modes to be excited in comparison with a single atom on the surface.<sup>8</sup> On the contrary, the obtained attempt frequency for the oxidized PCAT islands is close to the typical attempt frequency values reported for atoms on surfaces.<sup>9</sup>

On the basis of the evaluated diffusion parameters for the reduced and the oxidized PCAT on the hematite surface, the possibility to switch the morphologies of these islands was examined. Figure 5a shows the AFM micrograph of the oxidized islands on a hematite surface right after deposition, whereas Figure 5b shows the same sample (not at the same imaging location as Figure 5a) after its storage in a dry  $\text{N}_2$  atmosphere for about 4 months. Comparison of these two

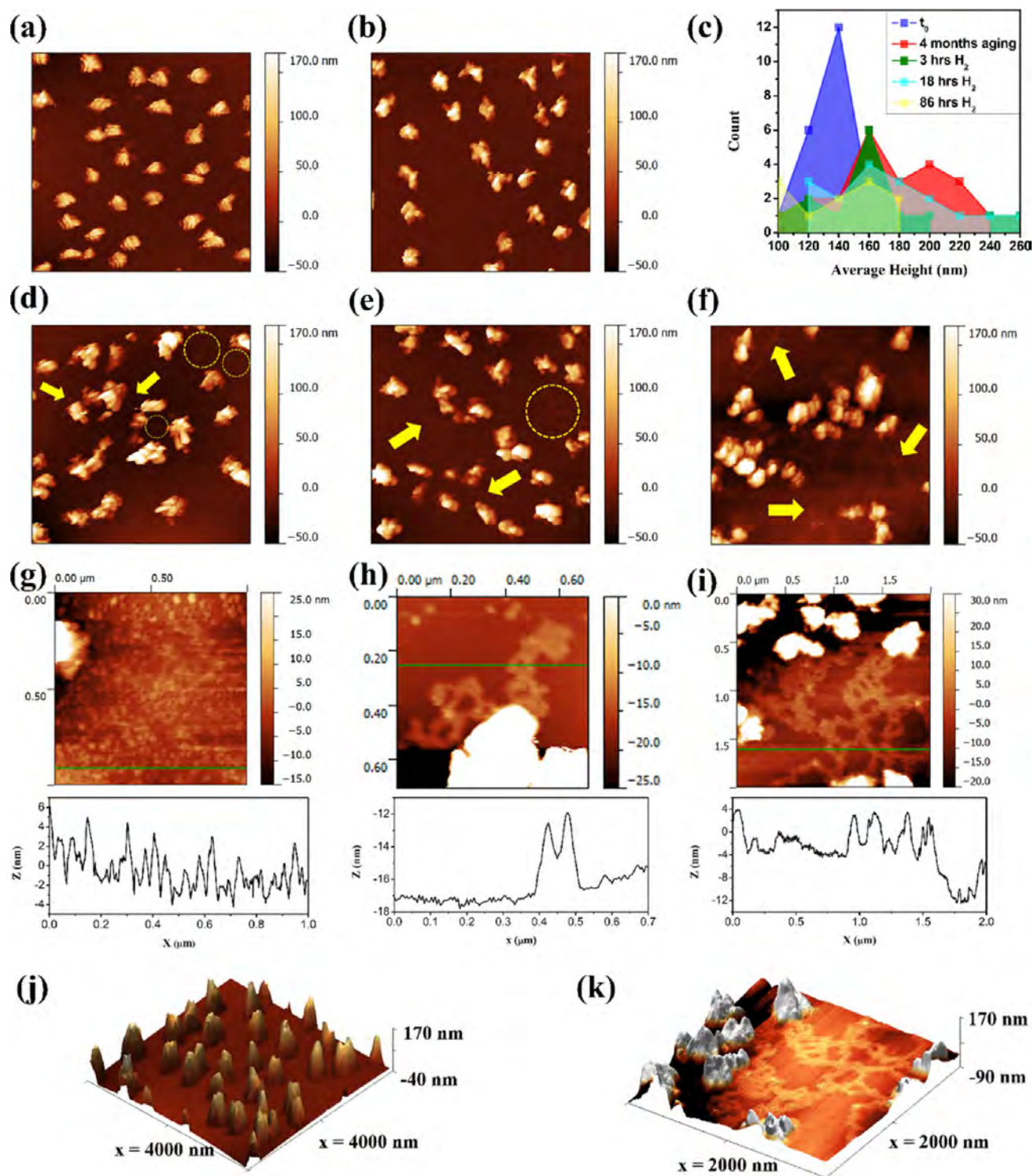


**Figure 5.** AFM micrographs of fully oxidized PCAT islands deposited on a hematite(1000) surface at room temperature (a) and the same sample after 4 months of aging in dry N<sub>2</sub> environment (b). (c) Height distribution of the islands in panels a, b and d–f. AFM of the sample in panel b after exposure to a hydrogen atmosphere for 3 (d,g), 18 (e,h), and 86 h (f,i). Panels g–i also show the height profile along the green line in the AFM micrographs. Panels a, b, and d–f are 4  $\mu\text{m}$   $\times$  4  $\mu\text{m}$ . (j) 3D view of the sample in panel a. (k) 3D view of a part of the sample in panel f.

Figures does not show discernible changes in the morphology of the islands. However, comparison of the height distribution of the islands (Figure 5c) in Figure 5a,b shows an increase in their height after storage in a dry environment for 4 months, indicating further dewetting of the surface by the oxidized PCAT during the storage time. Next, the sample was exposed

to a hydrogen-rich atmosphere to chemically reduce the oxidized PCAT islands. For this purpose the sample was placed in a reaction cell containing a vial of 100 mg of NaBH<sub>4</sub> in 1 mL of Millipore water (Figure S1). Figure 5d,–f shows the morphology of the PCAT islands after 3, 18, and 86 h of exposure to this atmosphere, respectively. Three hours of

exposure of the sample to this reducing atmosphere leads to an expansion of the islands (Figure 5d). This leads to a decrease in the number of islands with heights over 140 nm (Figure 5c). A closer look at the rim of these islands (Figure 5g) shows the presence of small particles with a height of  $\sim 5$  nm. A bare hematite surface exposed to the same environment for 3 h (Figure S2) lacks such structures, which shows that these particles are originating from the PCAT islands. Further exposure of this surface to the reducing environment for 18 h leads to the coexistence of smaller islands along the initial islands (Figure 5e) while the concentration of small organic particles at the rims of the primary islands increases (Figure 5h). Finally, 86 h of exposure of the sample to the reducing environment causes the collision of these islands with each other, indicating their displacement on the surface (Figure 5f). In addition, the smaller PCAT particles formed a continuous thin film between the primary islands (Figure 5i). These islands are more easily distinguished from the original oxidized islands in the 3D view of this sample in Figure 5k. The 3D view of the as-deposited oxidized islands on the hematite surface before exposure to a reducing atmosphere (Figure 5j) contains no trace of these smaller islands. Figure 5c shows that the average island heights do not drastically change by increasing the duration of exposure of PCAT islands to the hydrogen environment, but the total number of islands decreases. Instead, it results in an increase in the concentration of the small PCAT particles around the perimeter of the primary PCAT islands. This is consistent with the notion that the hydrogen gas mainly leads to the reduction of molecules on the outer surface of the oxidized PCAT islands. Considering the much higher attempt frequencies of the reduced PCAT in comparison with the oxidized PCAT, the reduced molecules at the rim of the islands can detach from the islands and diffuse on the surface of hematite, forming islands with thickness of  $\sim 5$  nm. This observation is consistent with a previous study of an electrochemical actuation measurement based on conducting polymers, showing the expansion of the redox polymer structures upon their reduction and their shrinkage due to their oxidation.<sup>32</sup>

**Nucleation and Growth of PCAT on Thermally Reduced Hematite.** To partially reduce the surface of a hematite single crystal, the hematite substrate was annealed in a vacuum environment. It has been shown that vacuum annealing of hematite at temperatures above 350 °C leads to the transformation of hematite to magnetite.<sup>33,34</sup> Therefore, the hematite substrate was annealed in two cycles under vacuum conditions (base pressure  $< 1 \times 10^{-8}$  Torr). The progress of the reduction process was monitored in situ by XPS. The Fe 2p<sub>1/2</sub> and Fe 2p<sub>3/2</sub> peaks of the pristine hematite substrate in Figure 6a are located at 724.7 and 710.8 eV, while its Fe 2p<sub>1/2</sub> and Fe 2p<sub>3/2</sub> shakeup satellite peaks are located at 733.1 and 724.7 eV. The location of these peaks in addition to the absence of the metallic Fe 2p peak is an indication of the presence of a pure phase of hematite on the surface of this sample.<sup>34</sup> In general, the position of the satellite peaks is monitored during the reduction or the oxidation of hematite. This is due to the more distinct shift of these peaks in comparison with the Fe 2p<sub>1/2</sub> and Fe 2p<sub>3/2</sub> peaks.<sup>34</sup> The Fe 2p spectrum of this sample after the first vacuum annealing cycle shows the shift of the two pairs of peaks mentioned above to lower BEs, which is an indication of transformation of Fe<sup>3+</sup> to Fe<sup>2+</sup>. These peaks shift further to lower BEs after the second annealing cycle, which is a sign of partial reduction of hematite by losing oxygen atoms from the

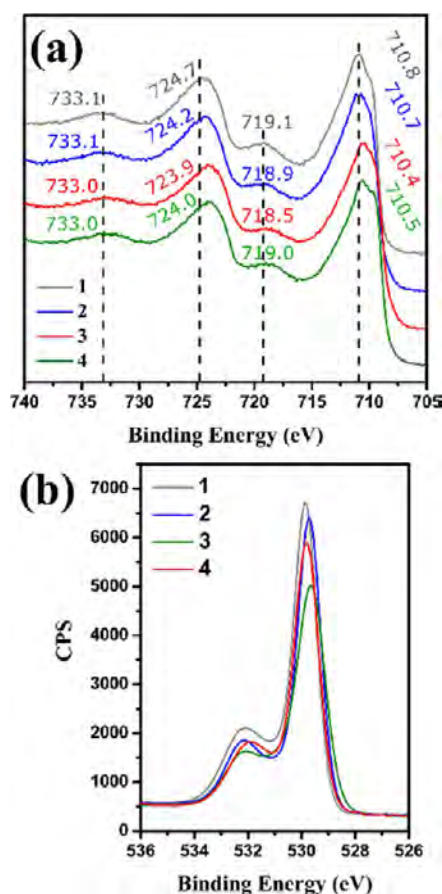


**Figure 6.** Partial reduction of hematite surface through vacuum annealing. High-resolution Fe 2p (a) and O 1s (b) XPS spectra of pristine hematite (1), 1st cycle of vacuum annealing (2), 2nd cycle of vacuum annealing (3), and after storage of the sample out of vacuum condition in dry Ar environment for 24 h (4).

surface. This is evident based on the continuous decrease in the intensity of the O 1s spectra of the annealed surfaces (Figure 6b, spectra 2 and 3) in comparison with the pristine hematite (Figure 6b, spectrum 1). The organic deposition chamber used in this work is not attached to the preparation (annealing) chamber, which requires the transfer of the partially reduced sample in an inert atmosphere (dry argon) between the two vacuum chambers. Therefore, it is necessary to examine the stability of the partially reduced hematite surface against oxidation in the absence of high vacuum conditions. Thus the sample was kept in a dry argon environment for 24 h before acquiring O 1s, Fe 2p, C 1s, and survey spectra of the sample. As it is evident in Figure 6a, the Fe 2p spectrum of this sample is slightly shifted to higher BEs, which is an indication of partial oxidation of the surface but not its full oxidation. The same conclusion can be drawn from the O 1s spectrum of this sample (Figure 6b), which shows a slight increase in its intensity in comparison with the partially reduced hematite surface obtained after the second vacuum annealing cycle.

To examine the effect of the substrate's oxidation state on PCAT islands growth, a hematite single crystal was annealed based on the above recipe. For each experiment the hematite single crystal was loosely clamped between two sapphire washers to avoid any thermal stress of the substrate, which could possibly change its surface roughness. The base pressure of the system was  $\sim 2 \times 10^{-7}$  Torr. After two cycles of

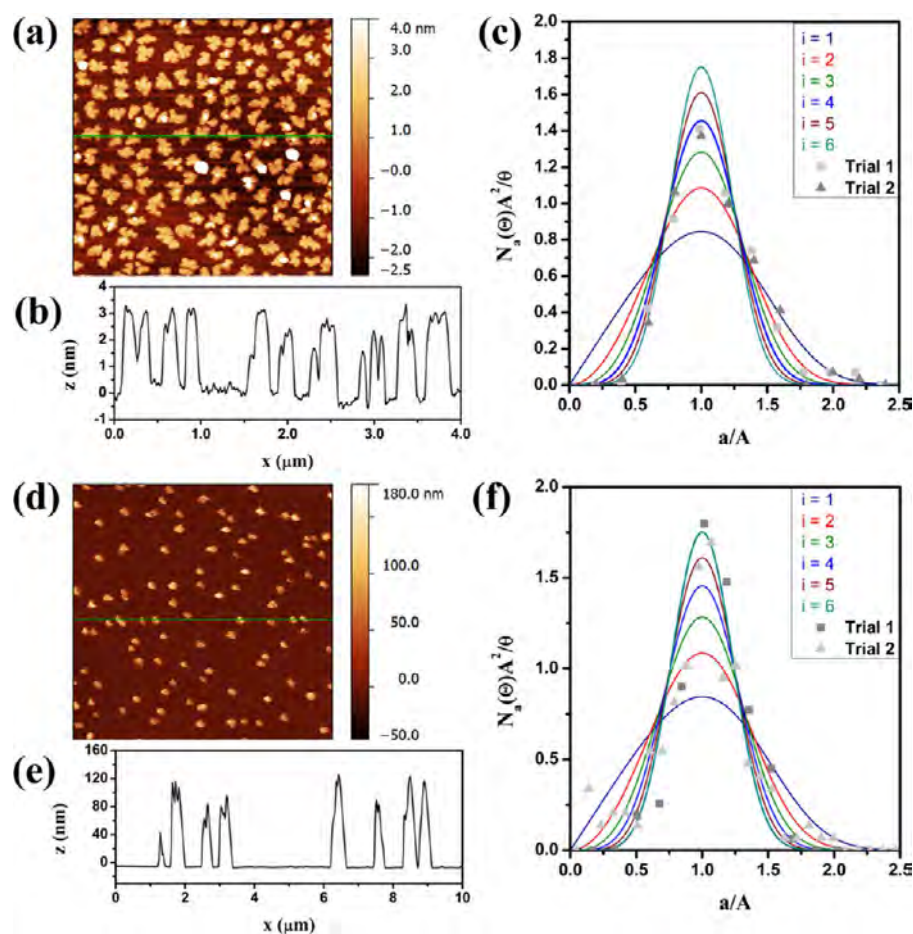


**Figure 7.** AFM images of the reduced (a,  $4 \mu\text{m} \times 4 \mu\text{m}$ ) and the oxidized (d,  $10 \mu\text{m} \times 10 \mu\text{m}$ ) islands on partially reduced hematite surface at 293 K. The cross-section of the heights of the reduced and the oxidized islands along the green lines in panels a and d are shown in panels b and e, respectively. (c,f) Scaling island size distribution of the reduced and the oxidized islands on partially reduced hematite, respectively.

annealing at 350 °C (5 min each), the sample was removed from the preparation chamber and quickly transferred into the deposition chamber under dry nitrogen. Figure 7a shows an AFM image of the reduced islands on a partially reduced hematite surface. The morphology of the islands does not show any noticeable difference to the reduced islands on a pristine hematite surface at 293 K (Figure 2). The cross-sectional height of the reduced islands on the partially reduced surface (Figure 7b) is  $\sim 3$  nm, which is comparable to the heights of the reduced islands on a pristine hematite surface (Figure 2). The effect of the oxidation state of the hematite substrate on the nucleation and growth of the reduced islands can be studied through their scaling island size distribution analysis. The scaling island size distribution of the reduced islands on partially reduced hematite is located in the proximity of  $f_i(u)$  for  $i = 4$ , which indicates that the critical island size for this system is close to four (Figure 7c). This is the same number of molecules (five molecules) required for the formation of a stable reduced island on pristine hematite surface. The same analysis was repeated for the oxidized islands on partially reduced hematite surface at 293 K. The AFM image of this sample (Figure 7d) does not show any differences in the morphology of these islands from the oxidized islands formed on pristine hematite surface at 293 K. The cross-section heights of these islands have maximum heights of  $\sim 120$  nm (Figure 7e) comparable to the heights of islands on a pristine hematite surface. The scaling size distribution of the oxidized islands on

the partially reduced surface of hematite (Figure 7f) fits best with  $f_i(u)$  for  $i = 5$ , which is the same critical island size (six molecules) for the oxidized islands on a pristine hematite surface. The partial reduction of the hematite substrate by removing the oxygen atoms from its surface sites does not appear to affect the nucleation and growth of different oxidation states of PCAT. Therefore, the oxidized PCAT might not be able to reoxidize the partially reduced surface of iron oxide until after it has settled down into islands.<sup>17</sup> The oxidation of the defect sites of the reduced iron oxide surfaces by the oxidized PCAT requires sufficient interaction between the organic molecules and the metal oxide surface. However, considering that the oxidized molecules dewet the surface, no effective interaction between the surface and the oxidized PCAT can take place. This will prevent the PCAT film from forming a uniform redox-active film for corrosion inhibition of steel.

## CONCLUSIONS

Thin films of two different oxidation states of PCAT on hematite(1000) single crystal surfaces were grown. The nucleation and growth of fully reduced and fully oxidized PCAT as a function of substrate temperature (278–338 K) have been studied. The nucleation density as a function of the substrate temperature has been evaluated for each of the two oxidation states of PCAT, which resulted in two linear fits. The absence of any bend in these two fits was interpreted as the dominance of a single growth mode. At low substrate

temperatures (<293 K) both types of oligoanilines formed compact islands on the surface. Increasing the substrate temperatures to 338 K significantly affected the growth of the reduced islands, leading to dendritic islands on the surface. However, high temperatures only had a minimal effect on the growth of the oxidized islands. In addition, at these substrate temperatures the height of the reduced islands was  $\sim 3$  nm, whereas for the oxidized islands this value was on average  $\sim 120$  nm. This significant difference between the heights of the islands of two oxidation states of an oligoaniline indicates better wetting of the iron oxide surface by the reduced state of PCAT and dewetting of the same surface by the oxidized form of this molecule. In addition, it was shown that the dewetting of the hematite surface by the oxidized molecules continues over time. Using the scaled island size distribution of the reduced and the oxidized molecules at room temperature it was found that the critical island sizes for the reduced molecules and the oxidized molecules are four and five, respectively. This means that five fully reduced molecules or six fully oxidized molecules are required for the formation of their respective stable islands. Furthermore, the activation energies for diffusion of the molecules away from the critical cluster for the reduced and the oxidized molecules on hematite surface were calculated to be about 1.30 and 0.55 eV, respectively. The attempt frequencies for surface diffusion of the fully reduced and the fully oxidized islands on hematite surface were calculated to be  $5 \times 10^{25}$  and  $5 \times 10^{11} \text{ s}^{-1}$ , respectively. The latter value is close to the attempt frequency for the surface diffusion of atoms ( $\sim 10^{11}$  to  $10^{13} \text{ s}^{-1}$ ). The former value is several orders of magnitude larger than the common preexponential factor for surface diffusion but still a realistic value.

It was also shown that the exposure of the oxidized islands to a reducing atmosphere ( $\text{H}_2$  gas) will lead to the chemical reduction of the outer surface of the islands. The higher diffusion prefactor of the reduced PCAT leads to the diffusion of these molecules away from the PCAT islands, forming a thin and continuous film of PCAT between the islands. Finally, it was shown that the change in the oxidation states of the substrate through partial reduction of the hematite surface does not affect the nucleation and growth of the reduced and the oxidized PCAT.

## ■ ASSOCIATED CONTENT

### Supporting Information

The Supporting Information is available free of charge on the ACS Publications website at DOI: 10.1021/acs.jpcc.7b08142.

Figure S1. Schematic depiction of sealed reaction cell for introduction of hydrogen gas to the surface of PCAT coated hematite surface. Figure S2. Bare hematite surface exposed to hydrogen-rich environment in Figure S1 for 3 h. (PDF)

## ■ AUTHOR INFORMATION

### Corresponding Author

\*E-mail: pkruse@mcmaster.ca. Tel: (905) 525-9140, ext. 23480. Fax: (905) 522-2509.

### ORCID

Peter Kruse: 0000-0003-4051-4375

### Notes

The authors declare no competing financial interest.

## ■ ACKNOWLEDGMENTS

We acknowledge technical assistance from Andrew D. Broomfield and Md. Omar Sharif. The National Science and Engineering Research Council of Canada (NSERC) provided financial support through the Discovery Grant program.

## ■ REFERENCES

- (1) Mishra, A.; Bäuerle, P. Small Molecule Organic Semiconductors on the Move: Promises for Future Solar Energy Technology. *Angew. Chem., Int. Ed.* **2012**, *51*, 2020–2067.
- (2) Wang, H.; Zhu, F.; Yang, J.; Geng, Y.; Yan, D. Weak Epitaxy Growth Affording High-Mobility Thin Films of Disk-Like Organic Semiconductors. *Adv. Mater.* **2007**, *19*, 2168–2171.
- (3) Xue, M.; Li, F.; Chen, D.; Yang, Z.; Wang, X.; Ji, J. High-Oriented Polypyrrole Nanotubes for Next-Generation Gas Sensor. *Adv. Mater.* **2016**, *28*, 8265–8270.
- (4) Mohtasebi, A.; Broomfield, A. D.; Chowdhury, T.; Selvaganapathy, P. R.; Kruse, P. Reagent-Free Quantification of Aqueous Free Chlorine via Electrical Readout of Colorimetrically Functionalized Pencil Lines. *ACS Appl. Mater. Interfaces* **2017**, *9*, 20748–20761.
- (5) Wang, Y.; Torres, J. A.; Stieg, A. Z.; Jiang, S.; Yeung, M. T.; Rubin, Y.; Chaudhuri, S.; Duan, X.; Kaner, R. B. Graphene-Assisted Solution Growth of Vertically Oriented Organic Semiconducting Single Crystals. *ACS Nano* **2015**, *9*, 9486–9496.
- (6) Hlawacek, G.; Puschnig, P.; Frank, P.; Winkler, A.; Ambrosch-Draxl, C.; Teichert, C. Characterization of Step-Edge Barriers in Organic Thin-Film Growth. *Science* **2008**, *321*, 108–111.
- (7) Campione, M.; Caprioli, S.; Moret, M.; Sassella, A. Homoepitaxial Growth of  $\alpha$ -Hexathiophene. *J. Phys. Chem. C* **2007**, *111*, 12741–12746.
- (8) Potocar, T.; Lorbek, S.; Nabok, D.; Shen, Q.; Tumbek, L.; Hlawacek, G.; Puschnig, P.; Ambrosch-Draxl, C.; Teichert, C.; Winkler, A. Initial Stages of a Para-Hexaphenyl Film Growth on Amorphous Mica. *Phys. Rev. B: Condens. Matter Mater. Phys.* **2011**, *83*, 1–10.
- (9) Venables, J. A.; Spiller, G. D. T.; Hanbücken, M. Nucleation and Growth of Thin Films. *Rep. Prog. Phys.* **1984**, *47*, 399–459.
- (10) Yang, J.; Wang, T.; Wang, H.; Zhu, F.; Li, G.; Yan, D. Ultrathin-Film Growth of Para-Sexiphenyl (1): Submonolayer Thin-Film Growth as a Function of the Substrate Temperature. *J. Phys. Chem. B* **2008**, *112*, 7816–7820.
- (11) Chowdhury, T.; Hoque, E.; Mohtasebi, A.; Kruse, P. Nature of the Interaction of N, N'-Diphenyl-1,4-Benzoquinonediimine with Iron Oxide Surfaces. *J. Phys. Chem. C* **2017**, *121*, 2721–2729.
- (12) Chowdhury, T.; Mohtasebi, A.; Kruse, P. Nature of the Interaction of N, N'-Diphenyl-1,4-Benzoquinonediimine with Iron Oxide Surfaces and Its Mobility on the Same Surfaces. *J. Phys. Chem. C* **2017**, *121*, 2294–2302.
- (13) Shao, Z.; Rannou, P.; Sadki, S.; Fey, N.; Lindsay, D. M.; Faul, C. F. J. Delineating Poly(Aniline) Redox Chemistry by Using Tailored Oligo(Aryleneamine)s: Towards Oligo(Aniline)-Based Organic Semiconductors with Tunable Optoelectronic Properties. *Chem. - Eur. J.* **2011**, *17*, 12512–12521.
- (14) Klinke, C.; Chen, J.; Afzali, A.; Avouris, P. Charge Transfer Induced Polarity Switching in Carbon Nanotube Transistors. *Nano Lett.* **2005**, *5*, 555–558.
- (15) Manseki, K.; Yu, Y.; Yanagida, S. A Phenyl-Capped Aniline Tetramer for Z907/tert-Butylpyridine-Based Dye-Sensitized Solar Cells and Molecular Modelling of the Device. *Chem. Commun.* **2013**, *49*, 1416–1418.
- (16) Dane, T. G.; Cresswell, P. T.; Bikondoa, O.; Newby, G. E.; Arnold, T.; Faul, C. F. J.; Briscoe, W. H. Structured Oligo(aniline) Nanofilms via Ionic Self-Assembly. *Soft Matter* **2012**, *8*, 2824–2832.
- (17) Mohtasebi, A.; Chowdhury, T.; Hsu, L. H. H.; Biesinger, M. C.; Kruse, P. Interfacial Charge Transfer between Phenyl-Capped Aniline Tetramer Films and Iron Oxide Surfaces. *J. Phys. Chem. C* **2016**, *120*, 29248–29263.

(18) Wei, Y.; Jamasbi, H.; Li, S.; Cheng, S.; Jansen, S. A.; Sein, L. T.; Zhang, W.; Wang, C. Corrosion Protection Properties of Coating of the Epoxy-Cured Aniline Oligomers Based on Spray and UV-Salt Fog Cyclic Tests. *ACS Symp. Ser.* **2003**, *843*, 208–227.

(19) Weßling, B. Passivation of Metals by Coating with Polyaniline: Corrosion Potential Shift and Morphological Changes. *Adv. Mater.* **1994**, *6*, 226–228.

(20) Ruiz, R.; Nickel, B.; Koch, N.; Feldman, L.; Haglund, R.; Kahn, A.; Family, F.; Scoles, G. Dynamic Scaling, Island Size Distribution, and Morphology in the Aggregation Regime of Submonolayer Pentacene Films. *Phys. Rev. Lett.* **2003**, *91*, 136102.

(21) Wang, W.; Macdiarmid, A. G. New Synthesis of Phenyl/Phenyl End-Capped Tetraaniline in the Leucoemeraldine and Emeraldine Oxidation States. *Synth. Met.* **2002**, *129*, 199–205.

(22) Nečas, D.; Klapetek, P. Gwyddion: An Open-Source Software for SPM Data Analysis. *Open Phys.* **2012**, *10*, 181–188.

(23) Fairley, N. *CasaXPS*, revision 2.3.17; Casa Software Ltd.: Teignmouth, Devon, 2016.

(24) Heeger, A. J. Semiconducting and Metallic Polymers: The Fourth Generation of Polymeric Materials (Nobel Lecture). *Angew. Chem., Int. Ed.* **2001**, *40*, 2591–2611.

(25) Thomas, J. O.; Andrade, H. D.; Mills, B. M.; Fox, N. A.; Hoerber, H. J. K.; Faul, C. F. J. Imaging the Predicted Isomerism of Oligo(aniline)s: A Scanning Tunneling Microscopy Study. *Small* **2015**, *11*, 3430–3434.

(26) Rebourt, E.; Joule, J. a.; Monkman, A. Polyaniline Oligomers; Synthesis and Characterisation. *Synth. Met.* **1997**, *84*, 65–66.

(27) Boyer, M.-I.; Quillard, S.; Rebourt, E.; Louarn, G.; Buisson, J. P.; Monkman, A.; Lefrant, S. Vibrational Analysis of Polyaniline: A Model Compound Approach. *J. Phys. Chem. B* **1998**, *102*, 7382–7392.

(28) Brune, H. Microscopic View of Epitaxial Metal Growth: Nucleation and Aggregation. *Surf. Sci. Rep.* **1998**, *31*, 125–229.

(29) Witten, T. A.; Sander, L. M. Diffusion-Limited Aggregation, a Kinetic Critical Phenomenon. *Phys. Rev. Lett.* **1981**, *47*, 1400–1403.

(30) Amar, J.; Family, F. Critical Cluster Size: Island Morphology and Size Distribution in Submonolayer Epitaxial Growth. *Phys. Rev. Lett.* **1995**, *74*, 2066–2069.

(31) Müllegger, S.; Winkler, A. Hexaphenyl Thin Films on Clean and Carbon Covered Au(1 1 1) Studied with TDS and LEED. *Surf. Sci.* **2006**, *600*, 1290–1299.

(32) Barisci, J. N.; Lewis, T. W.; Spinks, G. M.; Too, C. O.; Wallace, G. G. Conducting Polymers as a Basis for Responsive Materials Systems. *J. Intell. Mater. Syst. Struct.* **1998**, *9*, 723–731.

(33) Schlueter, C.; Lübke, M.; Gigler, A. M.; Moritz, W. Growth of Iron Oxides on Ag(111) — Reversible Fe<sub>2</sub>O<sub>3</sub>/Fe<sub>3</sub>O<sub>4</sub> Transformation. *Surf. Sci.* **2011**, *605*, 1986–1993.

(34) Xue, M.; Wang, S.; Wu, K.; Guo, J.; Guo, Q. Surface Structural Evolution in Iron Oxide Thin Films. *Langmuir* **2011**, *27*, 11–14.